Biodiversity Informatics, 19, 2025, pp. 86-108

REMOTE SENSING ENABLES ACCURATE ASSESSMENT OF FUNCTIONAL DIVERSITY RATHER THAN SPECIES DIVERSITY IN SANDY GRASSLANDS

Wen Li, Yu Peng*, and Xiaoyue Zhang

College of Life & Environmental Sciences, Minzu University of China, Beijing, China 100081

Abstract. The prediction of grassland plant diversity using satellite imagery has been the subject of intensive research. However, the accuracy of functional diversity (FD) predictions remains unclear. To address this, high-spatial-resolution WorldView-3 (WV-3) multispectral data were used to predict species diversity and FD at the pixel scale (1.2 × 1.2 m) in the central Hunshandak Sandland, Inner Mongolia, northern China. Data collected from 120 field plots (6 × 6 m) were employed to train and validate several statistical learning methods, with the primary objective of establishing links between 156 satellite-derived spectral and texture indices and 6 plant diversity indices. Among the various diversity indices tested, functional trait diversity—specifically Functional Attribute Diversity (FAD1) and Modified Functional Attribute Diversity (MFAD)—were predicted most effectively (with coefficients of determination of approximately 0.29 and 0.14, respectively; n=48) using texture indices. In contrast, species diversity (richness, H, E, or D) and other FD metrics were not well predicted by WV-3 data. Overall, WV data did not significantly improve the accuracy of plant diversity predictions in sandy grasslands. Additionally, high plot-level vegetation coverage was found to enhance the performance of spectral indices in predicting H, E, D, and FD. These results underscore the importance of accounting for variability across field conditions and demonstrate the potential of high-spatial-and-spectral-resolution satellite imagery for monitoring plant functional diversity in sandy grasslands.

Key words: Plant diversity, Species diversity, Functional diversity, Texture, Remote sensing, Sandy grassland

Introduction

The survival of both humans and animals depends on plant diversity (Radhamoni et al., 2023). Plant diversity can be measured at three different spatial scales: within-habitat diversity (α-diversity), between-habitat diversity (β-diversity), and regional diversity (γ-diversity) (Socolar et al., 2016). Species richness (R), Shannon-Wiener index (H), and Simpson index (D) are used to measure α diversity. Recently, leveraging the spectral characteristics and variations of different plant species, plant diversity has been assessed on a large scale using remote sensing techniques—exhibiting distinct advantages over traditional field measurement methods. Different plant species demonstrate different spectral traits.

The spectral species approach assumes that there are unique, definable spectral types ("spectral species") that can be distinguished in image processing, thus, facilitating biodiversity estimation (Rocchini & 2004; Féret & Asner, 2014). The linkage between species and "spectral species" can be validated using relatively simple to sophisticated spectral heterogeneity measures, which include measures of spectral entropy (Gillespie et al., 2008), statistical dispersion (Gould, 2000; Palmer et al., 2002), mean Euclidean distances between spectral clusters derived from principal components analysis (PCA) (Oldeland et al. 2010; Rocchini, 2007), and the use of first- and second-order image texture analysis (Culbert et al., 2012; Viedma, et al., 2012; Wood et al., 2013). The red (RED; 630-690nm) and near infrared (NIR; 760-900 nm) bands in the multi-spectral images are usually selected to assess species diversity (Schowengerdt, 2007; White et al., 2010; Peng et al 2019). Various spectral vegetation indices generated from multiple bands, such as Variation in Normalized Difference Vegetation Index (NDVI) (Gould, 2000; Bawa et al., 2002; Xu, 2004; Chawla et al., 2010, Kiran and Mudaliar, 2012), enhanced vegetation index (EVI) (Cabacinha, 2009; Gao X, 2000; Gallardo-Cruz et al., 2012), infrared index (IRI), middle infrared index (MIRI), atmospheric resistance vegetation index (ARVI), and soil adjusted vegetation index (SAVI) can predict plant diversity with considerable high accuracy (Nagendra, 2001; Bawa, et al., 2002; Schowengerdt, 2007; Cabacinha, 2009).

* *Corresponding author*: Yu Peng, yuupeng@163.com.

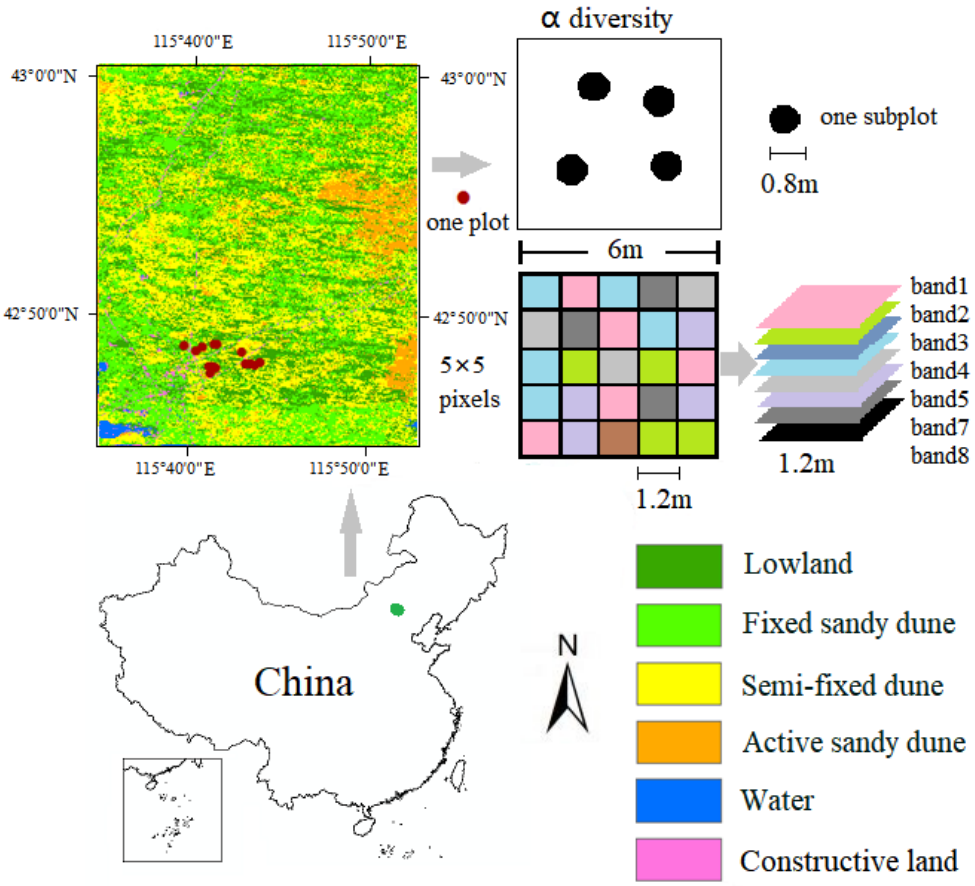

Fig. 1 Location of the study area, land use types, distribution of sampled plots and subplots in the field, and corresponding pixels in the WV-3 image of the study area. Each plot consists of 4 subplots (black circles) and corresponds to a 5×5 grid of WV-3 pixels.

Multispectral data from satellite platforms such as Landsat satellites (Sun et al., 2023; Mapfumo et al., 2016), the Sentinel series (Mpakairi et al., 2022; Xin et al 2024), QuickBird (Rocchini, 2007), WorldView series (Cho et al., 2012; Rocchini, 2007), SPOT series (Fauvel et al., 2020), and China′s Gaofen-3 and Haisi-1 satellites (Gu et al., 2024) have been widely used for vegetation monitoring and plant diversity estimation. The WV-3 satellite has eight visible near infrared (VNIR) bands (400–1040 nm) at 1.24 m resolution, has advantage in assessing plant diversity (Ferreira et al., 2016). The emergence of near-earth hyperspectral spectroscopy has addressed the scale mismatch between ground-based species information and earlier satellite-based multispectral monitoring (Schneider et al., 2017). Hyperspectral sensors offer the technical advantage of integrating fine spectral resolution with hundreds of spectral bands, improves the detection and identification of subtle differences at the plant species, functional, and genetic levels (Asner, 1998; Zhang et al., 2023).

Although species diversity has been extensively explored through remote sensing data, functional diversity (FD), i.e., diversity in plant species adaptation to survive in different environments and various strategies in reproduction, pollination processes, seed-dispersal methods and life forms (Ewers & Didham, 2006; Lindborg et al., 2012), has been rarely assessed using satellite-based high spatial and spectral resolution remote sensing imageries. FD is closely related to ecosystem service and ecological process, can also be regarded as an important indicator for biodiversity conservation (Diaz and Cabido, 2001). A plant's life form is one predictor for indicating the survival ability of plants in severely environment (Evju et al., 2015). Plants with suitable life forms will gradually replace unsuitable plants in a poor environment. For example, in plant communities in the arid environments such as deserts, shrubs and semi-shrubs increasingly substitute annual plants. Species with low offspring and colonization rates are easily influenced (Higgins et al., 2003; Henle et al., 2004) and therefore, dominant species in a community are usually highly adapted to suit their environments. Therefore, this study aimed to assess the ability of WV-3 data in assessing FD in the sandy grasslands of Hunshandak Sandland, by comparing the performances with those

of species diversity across various plot-level vegetation coverages.

Methods

Study area

This study was conducted in the temperate sandy grasslands of the Hunshandak Sandland (41°46′–43°69′ N, 114°55′–116°38′ E), located in Inner Mongolia, northern China (Fig. 1). The region has a temperate semi-arid climate, with an annual mean temperature of 1.7°C. The monthly diurnal minimum and maximum temperatures are -18.3°C and 18.7°C, respectively, and the annual precipitation ranges from 250 to 350 mm, 80–90% of which occurs between May and September (Wang, 2016a). The Hunshandak Sandland features a unique landscape comprising fixed sandy dunes, semi-fixed sandy dunes, mobile dunes, and lowlands, all of which support relatively rich plant diversity. The study area also includes other land cover types such as water ponds and constructed land. These diverse landscape elements, combined with the region′s relatively uniform elevation, make it an ideal site for testing the capacity of WV-3 data to assess both plant species diversity and functional diversity (FD) in sandy grasslands under complex background conditions.

Field sampling

Field surveys were conducted across 120 plots in the study area during July–August 2016, which corresponds to the peak growing season. Each plot (6 × 6 m, equivalent to a 5 × 5 grid of WV-3 pixels) was divided into four subplots, each with a diameter of 0.8 m (Fig. 1). In total, 480 subplots (corresponding to 480 WV-3 pixels), distributed across the 120 plots, were surveyed in this study. Global Positioning System (GPS) data were differentially corrected to achieve high-precision positioning within a geographic information system (GIS) environment.

Vascular plant species composition was recorded at the plot scale, with macroplot-level species lists compiled as the aggregated set of species identified across the four subplots within each plot. This nested sampling design for plot configuration has also been adopted in studies by Duccio Rocchini (2007) and Fauvel et al. (2020). All plants were identified to the species level, and the abundance of each species was recorded for each subplot. Details of the plot characteristics are provided in Table S1 in the Appendix.

Plant species diversity

In July and August 2016, the abundance, cover, and height of each plant species, as well as habitat categories (fixed sandy dunes, semi-fixed sandy dunes, mobile sandy dunes, lowlands, water bodies, and constructed land), were recorded. For each subplot, the number of individuals was counted for species whose stems were either fully or partially within the subplot. For clonal species, individuals were considered separate if their stems or culms were more than 20 cm apart from others of the same species. Canopy cover of all species within the subplot was visually estimated, and consistency in these visual estimates was ensured by having the same observer (Y. Peng) conduct all assessments across plots.

Based on the collected data on plant species abundance, four biodiversity indices were calculated: Richness (the number of plant species in a subplot), the Shannon–Wiener index (H), Simpson's species evenness index (D), and the Pielou index (E) (Magurran, 2004), using formulae (1)–(3).

$$H = -\sum_{i=1}^{s} \frac{n_i}{N} \ln \frac{n_i}{N} \quad (1),$$

where n_i is the number of individuals of the ith species, N is the total number of individuals of all the species, and ln is the natural logarithm. The value of H ranges from 0, meaning only one species is present, to 4.6, signifying high species richness and also signifying that different species in the quadrat or a community are equally abundant (Magurran, 2004).

$$D = 1 - \sum_{i=1}^{s} \left(\frac{n_i}{N}\right)^2 \quad (2)$$

The values of the Simpson species evenness index range from 0 (completely uneven) to 1 (different species occur in equal numbers).

$$E = H/\ln S \quad (3),$$

where S is the total number of species recorded (γ diversity) and H is the Shannon–Wiener index.

The plant diversity and dominant species of study plots are listed in Table S1 in the Appendix.

Functional trait diversity

Functional traits recorded for each species included life form (annual, biennial, perennial grass, shrub, or woody plant), seed dispersal method (gravitational, regular, wind, or animal-mediated), pollination mode (self-pollination, wind-pollination, or insect-pollination), flowering period (in months), flower longevity (in days), photosynthetic pathway (C_3, C_4, or CAM), and nitrogen-fixing ability (N-fixing or non-N-fixing). Based on these multiple functional traits, seven plant functional diversity (FD) indices were calculated using the FDiversity package (Casanoves et al., 2011; Spasojevic et al., 2014): Functional Attribute Diversity (FAD1), Modified Functional Attribute Diversi-

ty (MFAD), rRao, functional evenness (FEve), functional divergence (FDiv), functional dispersion (FDis), and functional specialization (FSpe). FAD1 represents the number of distinct attribute combinations present in the community, with values always less than or equal to species richness. MFAD is a modified index calculated as the sum of standardized distances between all pairs of species in trait space. rRao is derived from ultrametric trait distances and the abundance distribution of species within the community. FEve measures the regularity of spacing between species in trait space. FDiv quantifies the spread of trait values across the range of the trait space.
FDis is a multidimensional index based on multi-trait dispersion. FSpe, associated with threat categories, quantifies the average distinctiveness of all threatened species. The calculation formulas for each FD index are detailed in Casanoves et al. (2011).

Satellite image acquisition

A cloud-free WorldView-3 (WV-3, DigitalGlobe, Inc.) image covering the study area was acquired on 12 September 2015 (Fig. 1). At this time, most grasses remained leafy, making them easily distinguishable in the imagery due to their strong contrast with the surrounding sandy terrain. The WV-3 dataset included a panchromatic image with a spatial resolution of 0.30 m, accompanied by a multispectral image with a 1.20 m spatial resolution, spanning 8 spectral bands: coastal blue (427 nm), blue (482 nm), green (547 nm), yellow (604 nm), red (660 nm), red-edge (723 nm), near-infrared 1 (824 nm), and near-infrared 2 (914 nm). The WV-3 data were delivered at Level 2A. WV-3 data processing followed the methods described by Lelong et al. (2020) and Cerrejón et al. (2023). First, radiometric calibration was performed to convert digital numbers to absolute radiance using the gain and offset values for each spectral band. Next, absolute radiance was converted to top-of-atmosphere (TOA) reflectance, and the data were orthorectified to correct geometric distortions while minimizing topographical effects. Finally, the multispectral image was fused with the panchromatic image to generate a pansharpened multispectral image with a resolution of 0.30 m.

Spectral and textural analysis

This study assessed plant species diversity and functional trait diversity based on the spectral diversity theory, which posits that higher spectral diversity corresponds to greater plant diversity. Numerous studies have shown that dispersion metrics, such as the coefficient of variation (CV), serve as simple yet effective indicators of spectral heterogeneity within a sampling unit (e.g., an image window or kernel) (Anderson et al., 2009; Duro et al., 2014; Levin et al., 2007; Lucas & Carter, 2008). Here, we used the CV to link spectral heterogeneity within 5×5 image pixels to field-measured species diversity and functional diversity (FD) at each plot.

Before conducting the calculations, an NDVI threshold of ≥0.2 was applied to distinguish vegetation from desert areas, in accordance with the method proposed by Xin et al. (2024). First, 35 spectral indices (Table S2 in the Appendix; details are provided in the ENVI manual) were calculated at the pixel level using ENVI software. Second, for each spectral index, the CV (cv), mean value (mean), majority (maj), and variance (var) were computed using all pixels within a plot, yielding 140 spectral diversity values at the plot level. This approach allowed us to quantify the spectral diversity of each plot. Finally, spectral diversity values derived from all pixels within the plots were compared with field-measured species diversity and FD data. Image texture metrics, derived from multi-scale spectral values, are effective predictors of plant species richness. In this study, we also computed spectral texture values for each plot. In image texture analysis, the value of a central pixel within a moving window is determined by the spectral variability of its neighboring pixels (Hall-Beyer, 2017). We calculated one first-order texture metric and six second-order (_sec) texture metrics: angular second moment (mom), contrast (cont), dissimilarity (dis), homogeneity (hom), entropy (ent), and correlation (corr, _cor). These metrics were derived from panchromatic images and principal components (PCs) of multispectral images, where the PCs were obtained via principal component analysis (PCA) of the eight spectral bands. Second-order textures are based on the gray-level co-occurrence matrix, thus accounting for the spatial arrangement and relationships among neighboring pixels (Farwell et al., 2020). Detailed descriptions of these image texture metrics are available in the ENVI software manual. A single moving window size (5×5 pixels, corresponding to 6×6 m²) was selected for the analysis, as texture metrics across different window sizes are highly correlated and exhibit similar relationships with plant species richness (St-Louis et al., 2006; Culbert et al., 2012). Additionally, the CV (cv), mean (mean), majority (maj), and variance (var) of the PCs were calculated for each plot. In total, 140 spectral indices, 12 texture indices, and 4 PC indices were computed for each plot.

Statistical analysis

Of the 120 plots, five were excluded as their pixels primarily covered shifting sandy land. We employed

a two-step approach to explore the potential of spectral and texture indices for assessing plant diversity. The first step involved selecting indices with significant Pearson′s correlation coefficients using 67 plots. The second step validated these selected indices across different vegetation coverages using the remaining 48 plots. Pearson′s correlation coefficients were used to evaluate relationships between plant species diversity, functional trait diversity indices, and spectral/texture indices derived from satellite imagery. This provided an assessment of the potential of these spectral indices and texture metrics for estimating plant diversity or functional diversity. Spectral indices or texture metrics were considered optimal if they showed a statistically significant association ($P < 0.05$) with plant diversity indices based on Pearson′s correlation analysis.

Potential indices that exhibited significant relationships with plant diversity were designated as final optimal indices only if they passed the validation test. For this test, the remaining 48 randomly selected plots were used for model validation. The potential spectral indices were required to show high consistency in predicting plant diversity across different plant communities. We used vegetation coverage to examine its influence on the consistency of the selected indices in estimating plant diversity. Plot-level vegetation coverage was categorized into three classes based on values: 0–15%, 16–26%, and 27–100%, representing low, moderate, and high community coverage, respectively.

The performance of the selected indices in the validation test was evaluated using two metrics derived from the validation dataset: the correlation coefficient (r) and the significance level (p) between predicted and observed richness values. Indices with the highest r and $P < 0.01$ were deemed the best predictors.

Additionally, cluster analysis was used to identify groups of indices with similar performance, aiming to explore the underlying mechanisms of the best-performing indices in assessing plant diversity. These groups were not predefined prior to the analysis, and no a priori assumptions were made regarding the distribution of variables (indices). The indices were z-transformed for the analysis, and results are presented as a dendrogram, with groupings based on a squared Euclidean distance matrix.

Results

Cluster tree

The top 51 spectral and texture indices, which exhibited the highest number of significant correlations ($P < 0.05$) with plant diversity were clustered into five distinct groups (Fig. 2). Indices showing significant positive correlations with the species diversity indices (D, H) and the functional diversity index (FAD1) included correlation (corr), principal component correlation (pca-cor), variance (var), principal component variance (pca-var), entropy (ent), principal component entropy (pca-ent), dissimilarity (dis), contrast (cont), principal component dissimilarity (pca-dis), and principal component contrast (pca-con). These indices all belong to image texture measures. Notably, spectral indices based on spatial variability (e.g., coefficient of variation [CV], such as evi-cv) showed no significant relationships with species or functional diversity indices.

Indices with the most significant relationships were identified as potential optimal indices and selected for model construction and validation. Based on this criterion, corr, pca-cor, var, and pca-var were chosen as potential indices for further analysis.

Model development

Six texture and spectral indices that passed the aforementioned tests were retained for model development. The resulting models exhibited high coefficients of determination (R^2) and significant relationships between the indices and plant diversity indices ($P < 0.05$), indicating their potential as optimal indices (Table 1). Among these models, Simpson′s index (D) was significantly predicted by variance (var), correlation (Corr), principal component variance (PCA-var), principal component correlation (PCA-cor), and var-mean. All functional diversity (FD) indices—Functional Attribute Diversity (FAD1), Modified Functional Attribute Diversity (MFAD), and functional specialization (FSpe)—were significantly predicted by variance (var), correlation (Corr), principal component variance (PCA-var), and principal component correlation (PCA-cor).

Model validation

Using the six identified optimal spectral and texture indices listed in Table 1, plant diversity indices were calculated for the 48 model validation plots using the spectral and texture dataset. At the plot level, linear correlations between diversity estimates derived from spectral and texture indices and field-surveyed diversity were analyzed (Fig. 3). The six selected spectral and texture indices were further compared in terms of the consistency of their relationships with plant species or functional diversity across different vegetation coverage classes (0–15%, 16–26%, and 27–60%). Indices that exhibited significant correlations across all vegetation coverage classes were designated as the best-performing indices.

All models showed non-significant correlations ($P > 0.05$) between recorded and predicted plant diversi-

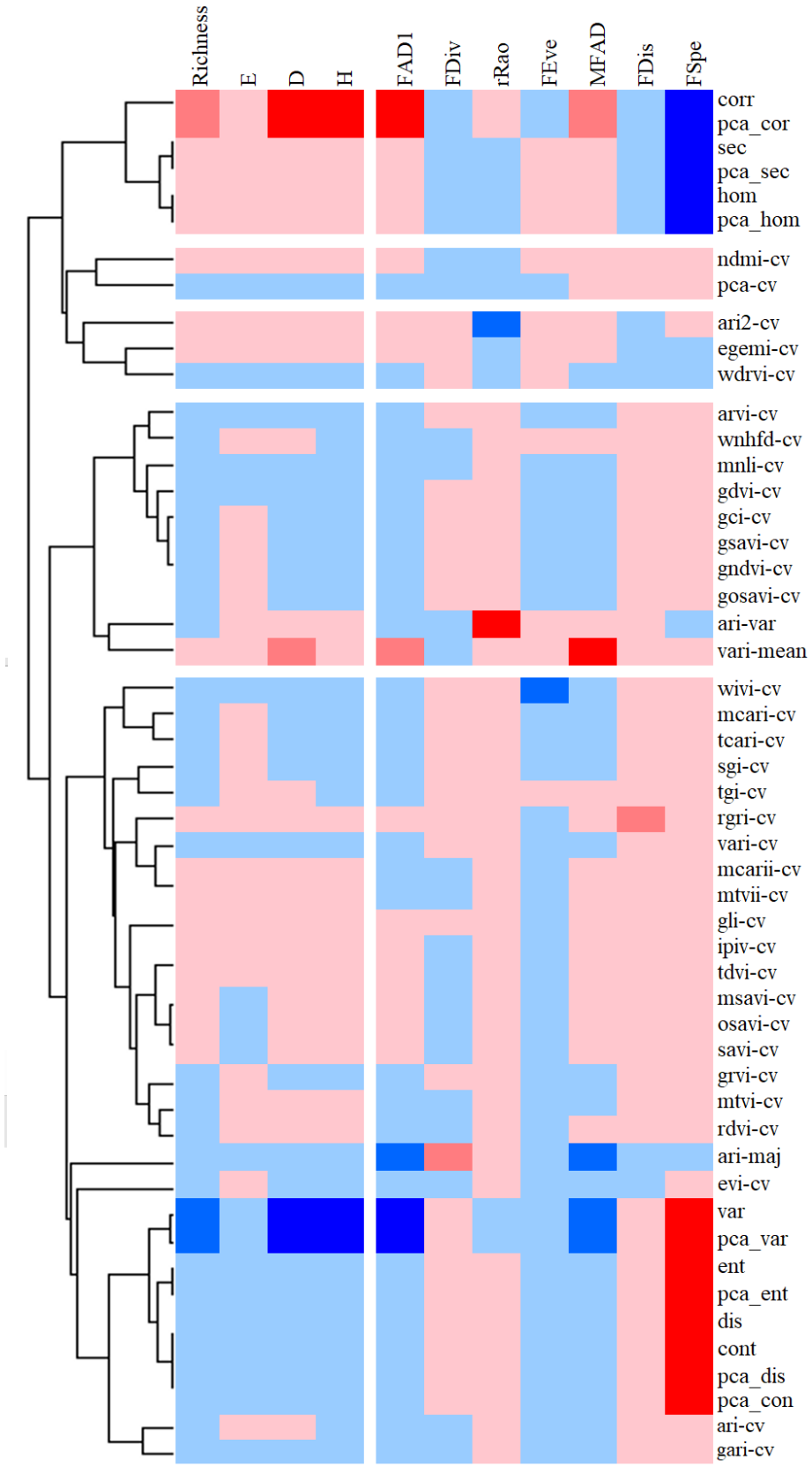

Fig. 2 Cluster dendrogram showing Pearson's correlation coefficients between spectral/texture indices and plant diversity indices. Deep red and blue indicate significant positive and negative correlations, respectively ($P < 0.05$); light colors indicate non-significant correlations ($P \geq 0.05$).

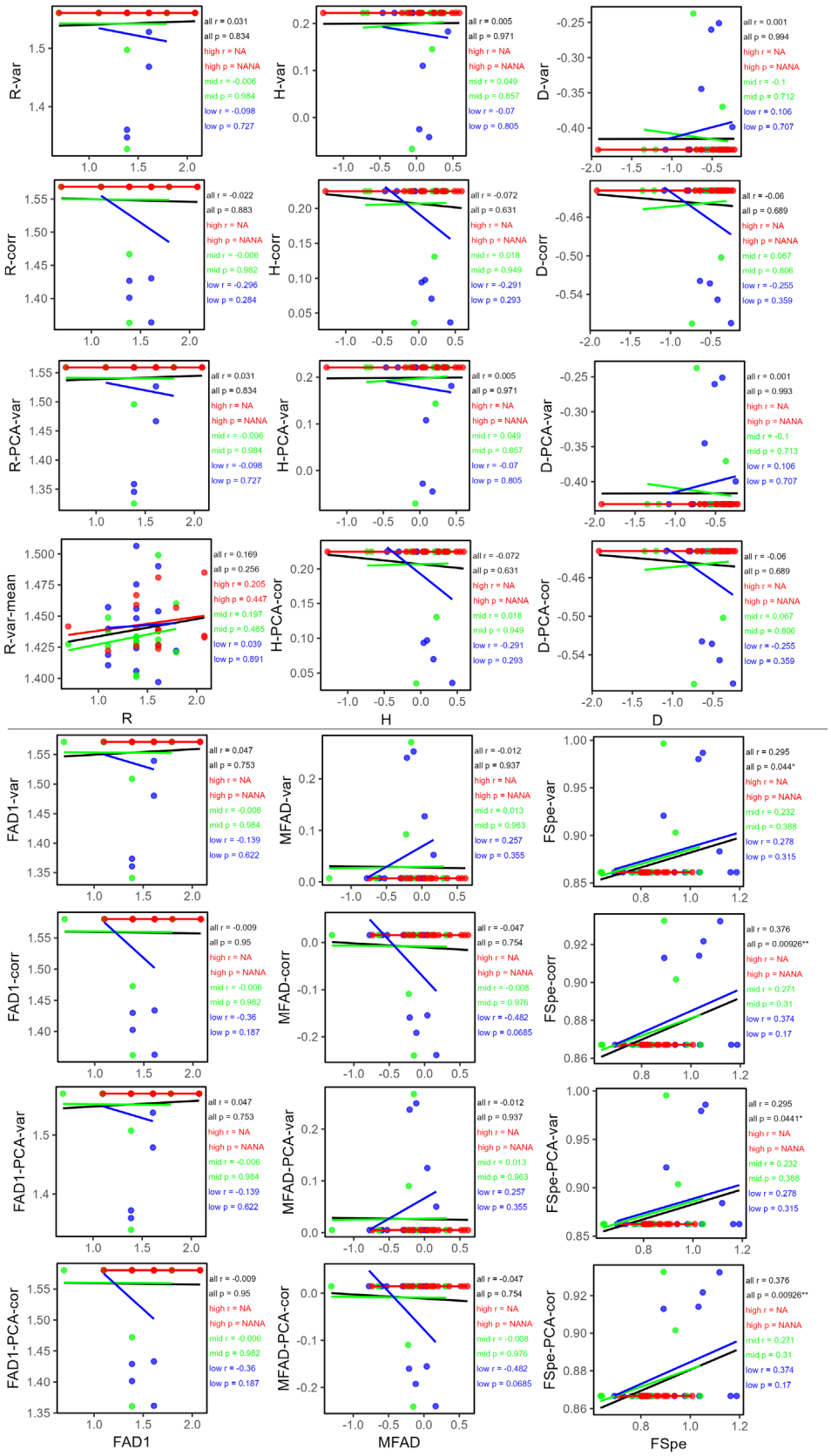

Fig. 3 Linear regressions between the natural log-transformed field-measured values (x-axis) and natural log-transformed predicted values (y-axis) for plant species diversity and functional diversity, using the validation dataset from the central Hunshandak Sandland, northern China. Predicted values were derived from the best-performing models listed in Table 1. "low," "mid," and "high" indicate plot-level vegetation coverage classes of 0–15%, 16–26%, and 27–60%, respectively.

Table 1 Selected spectral indices, texture indices, models, and parameters for estimating plant species diversity and functional diversity using the training dataset

	Richness	H	D	FDA1	MFAD	FSpe
Var	$Y = 4.761-0.001x$	$Y = 1.249-0.000317x$	$Y = 0.650+0.00014x$	$Y = 4.814-0.001x$	$Y = 1.007+0.000307x$	$Y = 2.366+0.000346x$
	$R^2=0.048$, $P = 0.041$	$R^2=0.081$, $P = 0.011$	$R^2=0.094$, $P = 0.007$	$R^2=0.061$, $P = 0.025$	$R^2=0.053$, $P = 0.034$	$R^2=0.183$, $P = 0.000$
Corr	$Y = 3.947+0.852x$	$Y = 1.046+0.206x$	$Y = 0.569+0.08x$	$Y = 3.945+0.911x$	$Y = 0.797+0.219x$	$Y = 2.534-0.154x$
	$R^2=0.074$, $P = 0.026$	$R^2=0.072$, $P = 0.016$	$R^2=0.061$, $P = 0.025$	$R^2=0.076$, $P = 0.014$	$R^2=0.059$, $P = 0.027$	$R^2=0.068$, $P = 0.021$
PCA-var	$Y = 4.755-0.001x$	$Y = 1.247-0.000318x$	$Y = 0.649+0.000141x$	$Y = 4.807-0.001x$	$Y = 1.005+0.000305x$	$Y = 2.369+0.00034x$
	$R^2=0.047$, $P = 0.044$	$R^2=0.079$, $P = 0.012$	$R^2=0.093$, $P = 0.007$	$R^2=0.059$, $P = 0.028$	$R^2=0.051$, $P = 0.038$	$R^2=0.172$, $P = 0.000$
PCA-cor	-	$Y = 1.045+0.207x$	$Y = 0.569+0.080x$	$Y = 3.941+0.915x$	$Y = 0.796+0.219x$	$Y = 2.534-0.155x$
		$R^2=0.071$, $P = 0.016$	$R^2=0.06$, $P = 0.025$	$R^2=0.076$, $P = 0.015$	$R^2=0.059$, $P = 0.028$	$R^2=0.068$, $P = 0.021$
Ari-maj	-	-	-	-	-	-
Var-mean	$Y = 3.944+0.855x$	-	$Y = 0.534+0.346x$	-	-	-
	$R^2=0.06$, $P = 0.026$		$R^2=0.065$, $P = 0.021$			

ty indices, except for the correlations between Modified Functional Attribute Diversity (MFAD) and four texture indices, and between variance (var) and Simpson′s index (D) (Fig. 3). When comparing correlation coefficient (r) values across vegetation coverage classes, all spectral and texture models exhibited similarly high r values (>0.2) for high-coverage plots (>27%), followed by low-coverage plots, while models for medium-coverage plots had the lowest r values. Among functional diversity indices, MFAD was most effectively predicted by the selected texture indices.

Discussion

Among the 156 spectral indices and texture metrics, only four performed relatively well in estimating plant species diversity and functional diversity (FD). These four indices were primarily texture measures: variance (var), principal component variance (PCA-var), var-mean, and correlation (corr). These indices, which reflect canopy structure and functional traits, can effectively indicate FD in sandy grasslands. Notably, leaf traits related to light capture and growth—such as photosynthetic pigments, nutrients, and leaf mass—primarily absorb and scatter light in the 350–700 nm spectral range (Ollinger, 2011). In contrast, secondary metabolites (e.g., lignin, cellulose, phenols, and tannins), which contribute to foliar defense and longevity, actively absorb and scatter near-infrared (NIR) and shortwave infrared (SWIR) radiation (Kokaly et al., 2009). This may partially explain why spectral indices show stronger associations with plant FD than with species diversity. Previous studies have observed that visible spectrum (VIS) variability (e.g., captured by var, var-mean, and PCA-var) is significantly higher in sandy landscapes compared to moist or wetland environments (Somers et al., 2015).

The visible spectrum, dominated by pigment absorption and canopy structure, exhibits less variability among plant species but greater variability among functional traits (Kattenborn et al., 2017; Pacheco-Labrador et al 2022). Additionally, biomass variation—closely linked to life form, a key functional trait—is primarily explained by vegetation structure (Hernández-Stefanoni et al., 2014) and can be well-captured by texture metrics. In sandy grasslands, environmental conditions strongly drive functional differentiation and adaptation in plants. The NIR region, reflecting leaf cellular structure (which scatters most incident energy) and canopy biochemical traits (e.g., leaf nutrient content), can distinguish plant strategies such as C_3, C_4, or CAM photosynthesis, or N-fixing capacity (Castillo-Riffart et al., 2017; Pacheco-Labrador et al 2022). Collectively, these factors explain why FD, rather than species diversity, is better estimated by spectral and texture indices.

A pixel represents a discrete spatial unit containing multiple objects, and the proportion of mixed objects increases with coarser resolution. A study on species-spectral diversity relationships across spatial grains, using North American floristic data, showed that high spatial and spectral resolution imagery improves plant species diversity estimation accuracy (Rocchini et al., 2014). Coarser resolution data, however, suffer from mixed-pixel issues and are less sensitive to spatial complexity (Rocchini, 2007). Previous research has found that estimation accuracy improves when spectral pixel resolution is finer than the size of the target object (Gholizadeh et al., 2019; Lopatin et al., 2017; Wang et al., 2018). Finer spatial resolution, such as that of WV-3 imagery, enhances the representation of “pure” objects within sampling areas (Rocchini, 2007; Pacheco-Labrador et al 2022) and captures more detailed spectral information. Consequently, WV-3 images exhibited higher spectral variability in 6×6 m plots compared to Aster or Landsat ETM+ imagery, likely due to reduced pixel mixing and larger effective sampling size. WV-3′s high spectral resolution further strengthens its capacity to estimate plant diversity.

In this study, texture metrics were derived from principal components (PCs) generated via principal component analysis (PCA) of 12 spectral bands. PCs maximize variance and are non-spatial, and it can be assumed that the first two PCs from 12 bands likely correlate with the most variable top-of-canopy structural and chemical traits (Roth et al., 2016; Dahlin, 2016). Our results align with previous studies using image texture to distinguish vegetation structural patterns between habitats (Wood et al., 2012), which also reported weak relationships ($0.01 < R^2 < 0.3$). Other studies have confirmed that image texture metrics effectively characterize vegetation heterogeneity, including foliage height diversity (Wood et al., 2012), successional stage (Jakubauskas, 1997), and structural complexity (Guo et al., 2004)—consistent with the use of vegetation indices (e.g., NDVI, EVI) to quantify biophysical aspects of functional traits. Texture metrics from WV-3 can capture spatial variations in vertical structures of mixed grasslands under different grazing regimes (Guo et al., 2004), supporting the utility of medium-resolution image textures for detecting vegetation heterogeneity. We used 5×5 pixel windows to calculate texture metrics, a size well-suited for grassland ecosystems. A study on North American plant species richness found that spectral diversity explained little variance, whereas the spatial extent of sampling units (floras) explained much of the variance in plant diversity (Rocchini et al., 2014).

In the present study, correlations between observed and predicted values were weak. For plant species richness, the strongest predictor was PCA-var ($R^2 = 0.19$), which is lower than the spectral diversity indices ($R^2 = 0.4–0.6$) derived from airborne hyperspectral data (Wang et al., 2018). Two key limitations likely contribute to this weakness. First, strong noise from the desert background in the study area weakens the correlation between WV-3-derived spectral indices and plant diversity. Rocchini et al. (2010, 2017) noted that pixels should be at least as large as the sampling unit, particularly when using spectral heterogeneity to estimate local species diversity. Additionally, the trade-off between noise from high resolution and information loss from low resolution must be considered. We speculate that WV-3′s fine resolution may exacerbate this issue: in vegetation-rich areas, numerous pixels may capture small shade patches cast by canopies (Nagendra & Rocchini, 2008), while in sparse vegetation, pixels are dominated by strong desert signals—both reducing the perceived strength of vegetation signals. Second, vegetation indices like NDVI struggle to detect plant signals in desert-vegetation mosaics, making it difficult to extract vegetation texture from mixed spectra, especially with fixed thresholds used in preprocessing (Hernández-Stefanoni et al., 2014). In this study, an NDVI threshold of 0.2 was used to distinguish vegetation from desert, but this may have excluded small-stemmed plants. A study conducted in a subalpine grassland of the Italian Alps showed that spectral diversity calculated via the Spectral Angle Mapper (SAM) proved to be a more effective proxy for biodiversity within the same ecosystem—whereas the broader spectral diversity approach failed to estimate α-diversity (Imran et al., 2024). This finding suggests that introducing additional novel spectral indices may enhance the accuracy of plant diversity estimation (Cherif et al., 2023). In addition, remote sensing for assessing forest functional diversity has typically demonstrated high estimation accuracy (Cimoli et al., 2024; Zeng et al., 2023). For example, in a subtropical evergreen and deciduous broad-leaved mixed forest, airborne LiDAR-derived parameters were found to correlate well with *in situ* plot-level morphological data ($R^2 \geq 0.67$) (Zeng et al., 2023). Currently, improving the estimation accuracy of both species and functional diversity in grasslands remains a key challenge for future research.

Conclusion

We demonstrate that texture metrics derived from high-spatial-resolution satellite imagery effectively predict plot-level patterns of plant functional traits in sandy grasslands, highlighting their potential to capture environmental heterogeneity not detected by more conventional heterogeneity metrics. While positive correlations were observed between texture metrics and both plant species richness and functional diversity, these relationships varied across diversity indices and texture metrics. Notably, for the functional index MFAD, the relationship remained consistently significant and positive. Our results underscore the complexity of the heterogeneity-diversity relationship, emphasizing the need for further investigation into these relationships using different satellite data sources and across diverse ecosystems. We conclude that texture metrics show promise as a tool for modeling functional diversity—rather than species diversity—in areas with sparse vegetation.

Acknowledgements

We thank WN Zhang, FC Li, TT Yang, J Li, and C Ma for their field survey. This research was funded by the General Program of the National Natural Science Foundation of China (32271555).

Data and Code Availability

Data will be made available on request.

Competing Interests

The authors declare no conflict of interest.

References

Asner, G. P., 1998. Biophysical and biochemical sources of variability in canopy reflectance. Remote Sens. Environ. 64(3): 23–253. https://doi.org/10.1016/S0034-4257(98)00014-5

Asner, G. P., Martin, R. E., Ford, A. J., Metcalfe, D. J., and Liddell, M. J., 2009a. Leaf chemical and spectral diversity in Australian tropical forests. Ecol. Appl. 19: 236–253. https://doi.org/10.1890/08-0541.1

Bawa, K., Rose, J., Ganeshaiah, K. N., Barve, N., Kiran, M. C., and Umashanker, R., 2002. Assessing biodiversity from space: Example from Western Ghats, India. Conserv. Ecol. 6(1): 7. https://www.ecologyandsociety.org/vol6/iss1/art7/

Cabacinha, C. D., and de Castro, S. S., 2009. Relationships between floristic diversity and vegetation indices, forest structure and landscape metrics of fragments in Brazilian Cerrado. For. Ecol. Manag. 257: 2157–2165. https://doi.org/10.1016/j.foreco.2009.02.024

Carlson, K. M., Asner, G. P., Hughes, R. F., Ostertag, R., and Martin, R. E., 2007. Hyperspectral remote sensing of canopy biodiversity in Hawaiian lowland rainforests. Ecosystems 10: 536–549. https://doi.org/10.1007/s10021-006-9013-5

Casanoves, F., Pla, L., Di Rienzo, J. A., and Díaz, S., 2011. FDiversity: A software package for the integrated analysis of functional diversity. Methods Ecol. Evol. 2: 233–237. https://doi.org/10.1111/j.2041-210X.2010.00088.x

Castillo-Riffart, I., Galleguillos, M., Lopatin, J., and Perez-Quezada, A. J. F., 2017. Predicting vascular plant diversity in anthropogenic peatlands: comparison of modeling methods with free satellite data. Remote Sens. 9(7): 681–692. https://doi.org/10.3390/rs9070681

Castro-Esau, K. L., Sánchez-Azofeifa, G. A., and Rivard, B., 2006b. Comparison of spectral indices obtained using multiple spectroradiometers. Remote Sens. Environ. 103: 276–288. https://doi.org/10.1016/j.rse.2006.05.005

Ceccato, P., Gobron, N., Flasse, S., and Asner, G. P., 2002. Designing a spectral index to estimate vegetation water content from remote sensing data: Part I: Theoretical approach. Remote Sens. Environ. 82(2–3): 188–197. https://doi.org/10.1016/S0034-4257(02)00074-7

Cerrejón, C., Valeria, O., and Fenton, N. J., 2023. Estimating lichen α- and β-diversity using satellite data at different spatial resolutions. Ecol. Indic. 149: 110173. https://doi.org/10.1016/j.ecolind.2023.110173

Chawla, A., Kumar, A., Rajkumar, J., Singh, R. D. R., Thukral, A. K., and Ahuja, P. S., 2010. Correlation of multispectral satellite data with plant species diversity vis-à-vis soil characteristics in a landscape of Western Himalayan Region, India. Appl. Remote Sens. 1: 013503. https://doi.org/10.1117/1.3486043

Cherif, E., Feilhauer, H., Berger, K., Asner, G. P., Martin, R. E., Ollinger, S. V., Wessman, C. A., and Schmidtlein, S., 2023. From spectra to plant functional traits: Transferable multi-trait models from heterogeneous and sparse data. Remote Sens. Environ. 292: 113580. https://doi.org/10.1016/j.rse.2023.113580

Cho, M. A., Mathieu, R., Asner, G. P., Martin, R. E., Ford, A. J., Metcalfe, D. J., Liddell, M. J., and Hughes, R. F., 2012. Mapping tree species composition in South African savannas using an integrated airborne spectral and LiDAR system. Remote Sens. Environ. 125: 214–226. https://doi.org/10.1016/j.rse.2012.05.015

Cimoli, E., Lucieer, A., Malenovsk, Z., Woodgate, W., Janoutová, R., Turner, D., Asner, G. P., and Martin, R. E., 2024. Mapping functional diversity of canopy physiological traits using UAS imaging spectroscopy. Remote Sens. Environ. 302: 113958. https://doi.org/10.1016/j.rse.2024.113958

Culbert, P. D., Radeloff, V. C., St-Louis, V., Flather, C. H., Rittenhouse, C. D., Albright, T. P., Asner, G. P., and Martin, R. E., 2012. Modeling broad-scale patterns of avian species richness across the midwestern United States with measures of satellite image texture. Remote Sens. Environ. 118: 140–150. https://doi.org/10.1016/j.rse.2011.11.013

Diaz, S., and Cabido, M., 2001. Vive la difference: Plant functional diversity matters to ecosystem processes. Trends Ecol. Evol. 16: 646–655. https://doi.org/10.1016/S0169-5347(01)02224-5

Doğan, H. M., and Doğan, M., 2020. Understanding and modeling plant biodiversity of Nallıhan (A3-Ankara) forest ecosystem by means of geographic information systems and remote sensing. Doctoral Dissertation, Ankara University, Ankara, Turkey. Available from: https://openaccess.ankara.edu.tr/handle/20.500.12573/26455

Duro, D. C., Girard, J., King, D. J., Fahrig, L., Mitchell, S., Lindsay, K., and Tischendorf, L., 2014. Predicting species diversity in agricultural environments using Landsat TM imagery. Remote Sens. Environ. 144: 214–225. https://doi.org/10.1016/j.rse.2013.12.013

Evju, M., Blumentrath, S., Skarpaas, O., Stabbetorp, O. E., and Sverdrup-Thygeson, A., 2015. Plant species occurrence in a fragmented grassland landscape, the importance of species traits. Biodivers. Conserv. 24(3): 547–561. https://doi.org/10.1007/s10531-014-0847-2

Ewers, R. M., and Didham, R. K., 2006. Confounding factors in the detection of species responses to habitat fragmentation. Biol. Rev. 81: 117–142. https://doi.org/10.1017/S1464793105006950

Farwell, L. S., Elsen, P. R., Razenkova, E., Pidgeon, A. M., and Radeloff, V. C., 2020. Habitat heterogeneity captured by 30-m resolution satellite image texture predicts bird richness across the United States. Ecol. Appl. 30(8): e02157. https://doi.org/10.1002/eap.2157

Fauvel, M., Lopes, M., Dubo, T., Rivers-Moore, J., Frison, P.-L., Gross, N., and Ouin, A., 2020. Prediction of plant diversity in grasslands using Sentinel-1 and -2 satellite image time series. Remote Sens. Environ. 237: 111536. https://doi.org/10.1016/j.rse.2019.111536

Feilhauer, H., Faude, U., and Schmidtlein, S., 2011. Combining Isomap ordination and imaging spectroscopy to map continuous floristic gradients in a heterogeneous landscape. Remote Sens. Environ. 115: 2513–2524. https://doi.org/10.1016/j.rse.2011.05.020

Feilhauer, H., Thonfeld, F., Faude, U., He, K., Rocchini, D., and Schmidtlein, S., 2013. Assessing floristic composition with multispectral sensors: A comparison based on monotemporal and multiseasonal field spectra. Int. J. Appl. Earth Obs. Geoinf. 21: 218–229. https://doi.org/10.1016/j.jag.2012.11.005

Féret, J.-B., and Asner, G. P., 2014. Mapping tropical forest canopy diversity using high-fidelity imaging spectroscopy. Ecol. Appl. 24: 1289–1296. https://doi.org/10.1890/13-0897.1

Ferreira, M. P., Zortea, M., Zanotta, D. C., Shimabukuro, Y. E., and Filho, C. R. D. S., 2016. Mapping tree species in tropical seasonal semi-deciduous forests with hyperspectral and multispectral data. Remote Sens. Environ. 179: 66–78. https://doi.org/10.1016/j.rse.2016.04.025

Gallardo-Cruz, J. A., Meave, J. A., González, E. J., Lebrija-Trejos, E. E., Romero-Romero, M. A., Asner, G. P., Martin, R. E., and Hughes, R. F., 2012. Predicting tropical dry forest successional attributes from space: Is the key hidden in image texture? PLoS ONE 7(2): e30506. https://doi.org/10.1371/journal.pone.0030506

Gao, X., Huete, A. R., Ni, W. G., and Miura, T., 2000. Optical-biophysical relationships of vegetation spectra without background contamination. Remote Sens. Environ. 74: 609–620. https://doi.org/10.1016/S0034-4257(00)00103-3

Gholizadeh, H., Amani, M., Townsend, P. A., Zygielbaum, A. I., Helzer, C. J., Asner, G. P., Martin, R. E., and Ollinger, S. V., 2019. Detecting prairie biodiversity with airborne remote sensing. Remote Sens. Environ. 221: 38–49. https://doi.org/10.1016/j.rse.2018.10.030

Gillespie, T. W., Foody, G. M., Rocchini, D., Giorgi, A. P., and Saatchi, S., 2008. Measuring and modeling biodiversity from space. Prog. Phys. Geogr. 32: 203–221. https://doi.org/10.1177/0309133308094513

Gould, W., 2000. Remote sensing of vegetation, plant species richness, and regional biodiversity hotspots. Ecol. Appl. 10(6): 1861–1870. https://doi.org/10.1890/1051-0761(2000)010[1861:RSOVPS]2.0.CO;2

Gu, C., Liang, J., Liu, X. Y., Asner, G. P., Martin, R. E., Ford, A. J., Metcalfe, D. J., and Liddell, M. J., 2024. Application and prospects of hyperspectral remote sensing in monitoring plant diversity in grassland. Chin. J. Appl. Ecol. 35(5): 1397–1407. https://doi.org/10.13287/j.1001-9332.202405.024

Guisan, A., and Thuiller, W., 2005. Predicting species distribution: Offering more than simple habitat models. Ecol. Lett. 8: 993–1009. https://doi.org/10.1111/j.1461-0248.2005.00787.x

Hall-Beyer, M., 2017. GLCM Texture: A Tutorial v. 3.0, March 2017. University of Calgary, Calgary, Alberta, Canada. Available from: https://www.ucalgary.ca/hallbey/tutorial

He, K. S., Rocchini, D., Neteler, M., and Nagendra, H., 2011. Benefits of hyperspectral remote sensing for tracking plant invasions. Divers. Distrib. 17: 381–392. https://doi.org/10.1111/j.1472-4642.2011.00794.x

Hector, A., and Bagchi, R., 2007. Biodiversity and ecosystem multifunctionality. Nature 448: 188–190. https://doi.org/10.1038/nature05987

Henle, K., Davies, K. F., Kleyer, M., Margules, C., and Settele, J., 2004. Predictors of species sensitivity to fragmentation. Biodivers. Conserv. 13: 207–251. https://doi.org/10.1023/B:BIOC.0000025823.16415.69

Hernández-Stefanoni, J. L., Dupuy, J. M., Johnson, D. K., Birdsey, R., Tun-Dzul, F., Peduzzi, A., Asner, G. P., and Martin, R. E., 2014. Improving species diversity and biomass estimates of tropical dry forests using airborne LiDAR. Remote Sens. 6: 4741–4763. https://doi.org/10.3390/rs6064741

Higgins, S. I., Lavorel, S., and Revilla, E., 2003. Estimating plant migration rates under habitat loss and fragmentation. Oikos 101: 354–366. https://doi.org/10.1034/j.1600-0706.2003.12158.x

Imran, H. A., Sakowska, K., Gianelle, D., Rocchini, D., Dalponte, M., Scotton, M., and Vescovo, L., 2024. Assessing plant trait diversity as an indicator of species α- and β-diversity in a subalpine grassland of the Italian Alps. Remote Sens. Ecol. Conserv. 10: 328–342. https://doi.org/10.1002/rse2.370

John, R., Chen, J., Lu, N., Guo, K., Liang, C., Wei, Y., Asner, G. P., and Martin, R. E., 2008. Predicting plant diversity based on remote sensing products in the semi-arid region of Inner Mongolia. Remote Sens. Environ. 112(5): 2018–2032. https://doi.org/10.1016/j.rse.2007.12.014

Kattenborn, T., Fassnacht, F., Pierce, S., Lopatin, J., Grime, J. P., and Schmidtlein, S., 2017. Linking plant strategies and plant traits derived by radiative transfer modelling. J. Veg. Sci. 28: 42–49. https://doi.org/10.1111/jvs.12533

Kiran, G. S., and Mudaliar, A., 2012. Remote sensing & geo-informatics technology in evaluation of forest tree diversity. Asian J. Plant Sci. Res. 2(3): 237–242. https://doi.org/10.5958/2249-7429.2012.00041.1

Kokaly, R. F., Asner, G. P., Ollinger, S. V., Martin, M. E., and Wessman, C. A., 2009. Characterizing canopy biochemistry from imaging spectroscopy and its application to ecosystem studies. Remote Sens. Environ. 113(S1): S78–S91. https://doi.org/10.1016/j.rse.2008.10.017

Lelong, C. C. D., Tshingomba, U. K., and Soti, V., 2020. Assessing Worldview-3 multispectral imaging abilities to map the tree diversity in semi-arid parklands. Int. J. Appl. Earth Obs. Geoinf. 93: 102211. https://doi.org/10.1016/j.jag.2020.102211

Levin, N., Shmida, A., Levanoni, O., Tamari, H., and Kark, S., 2007. Predicting mountain plant richness and rarity from space using satellite-derived vegetation indices. Divers. Distrib. 13: 692–703. https://doi.org/10.1111/j.1472-4642.2007.00366.x

Lindborg, R., Helm, A., Bommarco, R., Heikkinen, R. K., Kuhn, I., Asner, G. P., Martin, R. E., and Ford, A. J., 2012. Effect of habitat area and isolation on plant trait distribution in European forests and grasslands. Ecography 35: 356–363. https://doi.org/10.1111/j.1600-0587.2011.06962.x

Lopatin, J., Fassnacht, F. E., Kattenborn, T., and Schmidtlein, S., 2017. Mapping plant species in mixed grassland communities using close range imaging spectroscopy. Remote Sens. Environ. 201: 12–23. https://doi.org/10.1016/j.rse.2017.05.034

Lucas, K., and Carter, G., 2008. The use of hyperspectral remote sensing to assess vascular plant species richness on Horn Island, Mississippi. Remote Sens. Environ. 112: 3908–3915. https://doi.org/10.1016/j.rse.2008.06.014

Magurran, A. E., 2004. Measuring Biological Diversity. Oxford: Blackwell Publishing. https://doi.org/10.1002/9780470996267

Mapfumo, R. B., Asner, G. P., Martin, R. E., Ford, A. J., Metcalfe, D. J., Liddell, M. J., Hughes, R. F., and Ostertag, R., 2016. The relationship between satellite-derived indices and species diversity across African savanna ecosystems. Int. J. Appl. Earth Obs. Geoinf. 52: 306–317. https://doi.org/10.1016/j.jag.2016.07.013

Mpakairi, K. S., Dube, T., Dondofema, F., Asner, G. P., Martin, R. E., Ford, A. J., Metcalfe, D. J., and Liddell, M. J., 2022. Spatial Characterization of Vegetation Diversity in Groundwater Dependent Ecosystems Using In-Situ and Sentinel-2 MSI Satellite Data. Remote Sens. 14: 2995. https://doi.org/10.3390/rs14132995

Nagendra, H., 2001. Using remote sensing to assess biodiversity. Int. J. Remote Sens. 22: 2377–2400. https://doi.org/10.1080/01431160110043459

Nagendra, H., and Rocchini, D., 2008. Satellite imagery applied to biodiversity study in the tropics: The devil is in the detail. Biodivers. Conserv. 17: 3431–3442. https://doi.org/10.1007/s10531-008-9457-0

Oldeland, J., Wesuls, D., Rocchini, D., Schmidt, M., and Jürgens, N., 2010. Does using species abundance data improve estimates of species diversity from remotely sensed spectral heterogeneity? Ecol. Indic. 10: 390–396. https://doi.org/10.1016/j.ecolind.2009.11.006

Oldeland, J., Dorigo, W., Wesuls, D., and Jürgens, N., 2010. Mapping bush encroaching species by seasonal differences in hyperspectral imagery. Remote Sens. 2: 1416–1438. https://doi.org/10.3390/rs2071416

Ollinger, S. V., 2011. Sources of variability in canopy reflectance and the convergent properties of plants. New Phytol. 189: 375–394. https://doi.org/10.1111/j.1469-8137.2010.03527.x

Palmer, M. W., Earls, P. G., Hoagland, B. W., White, P. S., and Wohlgemuth, T., 2002. Quantitative tools for perfecting species lists. Environmetrics 13: 121–137. https://doi.org/10.1002/env.507

Pacheco-Labrador, J., Migliavacca, M., Ma, X., Mahecha, M., Carvalhais, N., Weber, U., Asner, G. P., and Martin, R. E., 2022. Challenging the link between functional and spectral diversity with radiative transfer modeling and data. Remote Sens. Environ. 280: 113170. https://doi.org/10.1016/j.rse.2022.113170

Peng, Y., Fan, M., Bai, L., Sang, W., Feng, J., Zhao, Z., and Tao, Z., 2019. Identification of the best hyper-

spectral indices in estimating plant species richness in sandy grasslands. Remote Sens. 11: 588. https://doi.org/10.3390/rs11050588

Radhamoni, H. V. N., Queenborough, S. A., Arietta, A. Z. A., Asner, G. P., Martin, R. E., Ford, A. J., Metcalfe, D. J., and Liddell, M. J., 2023. Local- and landscape-scale drivers of terrestrial herbaceous plant diversity along a tropical rainfall gradient in Western Ghats, India. J. Ecol. 111(5): 1021–1036. https://doi.org/10.1111/1365-2745.14010

Rocchini, D., Dadalt, L., Delucchi, L., Neteler, M., and Palmer, M. W., 2014. Disentangling the role of remotely sensed spectral heterogeneity as a proxy for North American plant species richness. Community Ecol. 15(1): 37–43. https://doi.org/10.1080/17450979.2014.881461

Rocchini, D., 2007. Effects of spatial and spectral resolution in estimating ecosystem α-diversity by satellite imagery. Remote Sens. Environ. 111: 423–434. https://doi.org/10.1016/j.rse.2007.05.014

Rocchini, D., Balkenhol, N., Carter, G. A., Foody, G. M., Gillespie, T. W., He, K., Asner, G. P., and Martin, R. E., 2010. Remotely sensed spectral heterogeneity as a proxy for species diversity: Recent advances and open challenges. Ecol. Inform. 5: 318–329. https://doi.org/10.1016/j.ecoinf.2010.03.004

Rocchini, D., Chiarucci, A., and Loiselle, S. A., 2004. Testing the spectral variation hypothesis by using satellite multispectral images. Acta Oecol. 26: 117–120. https://doi.org/10.1016/j.actao.2004.03.005

Rocchini, D., Marcantonio, M., and Riccota, C., 2017. Measuring Rao′s Q diversity index from remote sensing: An open source solution. Ecol. Indic. 72: 234–238. https://doi.org/10.1016/j.ecolind.2016.10.021

Rocchini, D., Ricotta, C., and Chiarucci, A., 2007. Using satellite imagery to assess plant species richness: The role of multispectral systems. Appl. Veg. Sci. 10: 325–331. https://doi.org/10.1111/j.1654-109X.2007.00316.x

Roth, K. L., Casas, A., Huesca, M., Ustin, S. L., Alsina, M. M., Mathews, S. A., and Whiting, M. L., 2016. Leaf spectral clusters as potential optical leaf functional types within California. Remote Sens. Environ. 184: 229–246. https://doi.org/10.1016/j.rse.2016.08.015

Schmidtlein, S., Feilhauer, H., and Bruelheide, H., 2012. Mapping plant strategy types using remote sensing. J. Veg. Sci. 23: 395–405. https://doi.org/10.1111/j.1654-109X.2011.01230.x

Schneider, F. D., Morsdorf, F., Schmid, B., Asner, G. P., Martin, R. E., Ford, A. J., Metcalfe, D. J., and Liddell, M. J., 2017. Mapping functional diversity from remotely sensed morphological and physiological forest traits. Nat. Commun. 8: 1441. https://doi.org/10.1038/s41467-017-01532-8

Schowengerdt, R., 2007. Remote Sensing: Models and Methods for Image Processing. Oxford: Elsevier. 515 p. https://doi.org/10.1016/B978-012374372-1.00001-1

Socolar, J. B., Gilroy, J. J., Kunin, W. E., Asner, G. P., Martin, R. E., Ford, A. J., Metcalfe, D. J., and Liddell, M. J., 2016. How should beta-diversity inform biodiversity conservation? Trends Ecol. Evol. 31(1): 67–80. https://doi.org/10.1016/j.tree.2015.10.004

Somers, B., Asner, G. P., Martin, R. E., Anderson, C. B., Knapp, D. E., Wright, S. J., Ostertag, R., and Hughes, R. F., 2015. Mesoscale assessment of changes in tropical tree species richness across a bioclimatic gradient in Panama using airborne imaging spectroscopy. Remote Sens. Environ. 167: 111–120. https://doi.org/10.1016/j.rse.2015.06.032

Somers, B., Verbesselt, J., Ampe, E. M., Sims, N., Verstraeten, W. W., and Coppin, P., 2010b. Spectral mixture analysis to monitor defoliation in mixed aged *Eucalyptus globulus* Labill plantations in southern Australia using Landsat 5TM and EO-1 Hyperion data. Int. J. Appl. Earth Obs. Geoinf. 12: 270–277. https://doi.org/10.1016/j.jag.2010.01.006

Spasojevic, M. J., Grace, J. B., Harrison, S., and Damschen, E. I., 2014. Functional diversity supports the physiological tolerance hypothesis for plant species richness along climatic gradients. J. Ecol. 102: 447–455. https://doi.org/10.1111/1365-2745.12214

Sun, W., Liu, W., Wang, Y., Asner, G. P., Martin, R. E., Ford, A. J., Metcalfe, D. J., and Liddell, M. J., 2023. Progress and prospects of global hyperspectral remote sensing research on wetlands from 2010 to 2022. J. Remote Sens. 27(6): 1281–1299. https://doi.org/10.11834/jrs.20230374

Tuanmu, M. N., and Jetz, M., 2015. A global, remote sensing-based characterization of terrestrial habitat heterogeneity for biodiversity and ecosystem modeling. Global Ecol. Biogeogr. 24: 1329–1339. https://doi.org/10.1111/geb.12316

Vaglio Laurin, G., Chan, J. C.-W., Chen, Q., Lindsell, J. A., Coomes, D. A., Asner, G. P., Martin, R. E., and Ford, A. J., 2014. Biodiversity mapping in a Tropical West African forest with airborne hyperspectral data. PLoS ONE 9(6): e97910. https://doi.org/10.1371/journal.pone.0097910

Viedma, O., Torres, I., Pérez, B., and Moreno, J. M., 2012. Modeling plant species richness using reflectance and texture data derived from QuickBird in a recently burned area of central Spain. Remote Sens.

Environ. 119: 208–221. https://doi.org/10.1016/j.rse.2011.12.015

Wang, R., Gamon, J. A., Montgomery, R. A., and Townsend, P. A., 2016a. Seasonal variation in the NDVI–species richness relationship in a prairie grassland experiment (Cedar Creek). Remote Sens. 8: 128–131. https://doi.org/10.3390/rs8020128

Wang, R., Gamon, J. A., Cavender-Bares, J., Townsend, P. A., and Zygielbaum, A. I., 2018. The spatial sensitivity of the spectral diversity-biodiversity relationship: An experimental test in a prairie grassland. Ecol. Appl. 28: 541–556. https://doi.org/10.1002/eap.1724

White, J. C., Gómez, C., Wulder, M. A., and Coops, N. C., 2010. Characterizing temperate forest structural and spectral diversity with Hyperion EO-1 data. Remote Sens. Environ. 114: 1576–1589. https://doi.org/10.1016/j.rse.2010.02.018

Wood, E. M., Pidgeon, A. M., Radeloff, V. C., and Keuler, N. S., 2012. Image texture as a remotely sensed measure of vegetation structure. Remote Sens. Environ. 121: 516–526. https://doi.org/10.1016/j.rse.2012.02.020

Wood, E. M., Pidgeon, A. M., Radeloff, V. C., and Keuler, N. S., 2013. Image texture predicts avian density and species richness. PLoS ONE 8(5): e63211. https://doi.org/10.1371/journal.pone.0063211

Xin, J. X., Li, J. N., Zeng, Q. Q., Peng, Y., Asner, G. P., Martin, R. E., Ford, A. J., and Liddell, M. J., 2024. High-precision estimation of plant alpha diversity in different ecosystems based on Sentinel-2 data. Ecol. Indic. 166: 112527. https://doi.org/10.1016/j.ecolind.2024.112527

Zhang, Y. W., Guo, Y. P., Tang, R., Tang, Z. Y., Asner, G. P., Martin, R. E., Ford, A. J., and Liddell, M. J., 2023. Progress and trends of application of hyperspectral remote sensing in plant diversity research. Natl. Remote Sens. Bull. 27(11): 2467–2483. https://doi.org/10.11834/jrs.20231048

Zheng, Z., Schmid, B., Zeng, Y., Schuman, M. C., Zhao, D., Schaepman, M. E., Asner, G. P., and Martin, R. E., 2023. Remotely sensed functional diversity and its association with productivity in a subtropical forest. Remote Sens. Environ. 290: 113530. https://doi.org/10.1016/j.rse.2023.113530

Appendix

Table S1 Coverage, habitat type, plant diversity, and dominant species in study plots

Plotid	Coverage	Altitude	Habitat type	Richness	H	D	E	Dominant species
2	4	1331.0	Semi-fixed	3	0.80	0.45	0.72	*Salsola collina*
3	14	1330.0	Semi-fixed	3	0.76	0.43	0.70	*Ulmus pumila*
5	53	1334.0	Semi-fixed	4	1.13	0.63	0.81	*Polygonum divaricatum*
6	11	1329.0	Semi-fixed	5	1.09	0.53	0.67	*Salsola collina*
7	26	1328.0	Semi-fixed	3	0.78	0.45	0.71	*Polygonum divaricatum*
10	6	1329.0	Semi-fixed	4	0.96	0.51	0.69	*Salsola collina*
12	11	1330.0	Semi-fixed	4	1.28	0.69	0.92	*Salsola collina*
15	17	1323.0	Semi-fixed	5	1.46	0.74	0.91	*Polygonum divaricatum*
16	26	1323.4	Semi-fixed	8	1.71	0.78	0.82	*Potentilla supina*
17	9	1326.0	Semi-fixed	5	1.08	0.56	0.67	*Salsola collina*
18	20	1329.1	Semi-fixed	5	1.46	0.74	0.91	*Lappula myosotis*
19	25	1328.0	Semi-fixed	4	1.24	0.69	0.89	*Polygonum divaricatum*
20	8	1321.0	Semi-fixed	5	1.07	0.53	0.66	*Echinops davuricus*
21	8	1324.0	Semi-fixed	4	0.77	0.39	0.56	*Salsola collina*
22	5	1322.0	Semi-fixed	4	1.05	0.58	0.76	*Agropyron mongolicum*
23	4	1323.7	Semi-fixed	3	1.05	0.64	0.96	*Potentilla supina*
24	22	1324.0	Semi-fixed	5	1.43	0.74	0.89	*Polygonum divaricatum*
25	11	1322.0	Semi-fixed	6	1.59	0.77	0.89	*Phragmites australis*
26	40	1321.0	Semi-fixed	5	1.45	0.74	0.90	*Bromus ircutensis*
27	37	1321.0	Semi-fixed	4	1.08	0.62	0.78	*Potentilla supina*
28	12	1326.4	Semi-fixed	5	0.94	0.46	0.59	*Leymus chinensis*
29	27	1325.0	Semi-fixed	4	1.27	0.69	0.92	*Polygonum divaricatum*
30	13	1326.0	Semi-shift	3	0.96	0.59	0.87	*Artemisia ordosica*
31	15	1327.4	Semi-shift	4	1.05	0.60	0.76	*Artemisia ordosica*
32	22	1330.0	Semi-shift	2	0.68	0.49	0.98	*Artemisia ordosica*
33	10	1326.8	Semi-shift	3	0.63	0.34	0.57	*Leymus secalinus*
34	24	1329.0	Semi-shift	3	0.93	0.57	0.84	*Artemisia ordosica*
35	14	1325.0	Semi-shift	4	1.26	0.69	0.91	*Artemisia ordosica*
36	13	1323.3	Semi-shift	5	1.26	0.66	0.79	*Artemisia ordosica*
37	10	1324.0	Semi-shift	4	1.21	0.67	0.87	*Agropyron mongolicum*
38	11	1323.6	Semi-shift	4	1.24	0.68	0.89	*Artemisia ordosica*
39	15	1321.3	Semi-shift	3	0.95	0.56	0.86	*Polygonum divaricatum*
40	32	1324.0	Semi-shift	2	0.64	0.44	0.92	*Artemisia ordosica*
42	29	1323.0	Semi-shift	4	1.27	0.69	0.92	*Polygonum divaricatum*
43	9	1322.0	Semi-shift	6	1.37	0.66	0.76	*Agropyron mongolicum*
44	8	1322.0	Semi-shift	3	0.74	0.45	0.67	*Salsola collina*
45	14	1319.0	Lowland	5	1.49	0.75	0.93	*Agropyron mongolicum*
46	25	1322.5	Lowland	4	1.00	0.53	0.72	*Leymus secalinus*
47	25	1319.2	Lowland	6	1.38	0.69	0.77	*Leymus secalinus*
48	26	1319.0	Lowland	6	1.31	0.61	0.73	*Agropyron mongolicum*

49	27	1317.0	Lowland	3	0.82	0.53	0.74	*Carex duriuscula*
50	16	1320.0	Lowland	6	1.68	0.80	0.94	*Salsola collina*
51	45	1319.7	Lowland	5	1.27	0.67	0.79	*Carex duriuscula*
52	19	1319.0	Lowland	6	1.46	0.71	0.81	*Agropyron mongolicum*
53	34	1320.6	Lowland	7	1.17	0.54	0.60	*Agropyron mongolicum*
54	39	1322.0	Lowland	5	1.44	0.73	0.89	*Carex duriuscula*
55	10	1320.0	Lowland	5	1.38	0.70	0.85	*Artemisia ordosica*
56	85	1326.0	Lowland	7	1.55	0.73	0.80	*Agropyron mongolicum*
57	41	1318.7	Lowland	6	1.27	0.65	0.71	*Carex duriuscula*
58	20	1320.0	Lowland	4	1.06	0.59	0.77	*Agropyron mongolicum*
59	25	1319.4	Lowland	4	0.86	0.50	0.62	*Agropyron mongolicum*
60	38	1334.0	Fixed-land	4	1.03	0.61	0.74	*Leymus chinensis*
61	78	1328.0	Fixed-land	2	0.28	0.15	0.40	*Leymus secalinus*
62	23	1329.0	Fixed-land	2	0.53	0.35	0.76	*Leymus chinensis*
63	24	1329.3	Fixed-land	5	1.33	0.70	0.83	*Agropyron mongolicum*
64	16	1324.5	Fixed-land	4	1.21	0.67	0.87	*Corispermum stauntonii*
65	18	1326.4	Fixed-land	4	1.15	0.64	0.83	*Corispermum stauntonii*
66	14	1326.7	Fixed-land	3	1.06	0.64	0.96	*Artemisia ordosica*
67	31	1327.1	Fixed-land	5	1.32	0.68	0.82	*Carex duriuscula*
68	23	1326.1	Semi-fixed	4	1.18	0.65	0.85	*Artemisia ordosica*
69	13	1325.0	Fixed-land	4	1.12	0.61	0.81	*Corispermum stauntonii*
70	19	1324.4	Fixed-land	4	1.08	0.61	0.78	*Artemisia ordosica*
71	43	1326.3	Fixed-land	5	1.04	0.50	0.65	*Carex duriuscula*
72	42	1330.2	Semi-fixed	4	1.14	0.65	0.82	*Artemisia ordosica*
73	17	1327.6	Semi-fixed	3	0.92	0.57	0.84	*Artemisia ordosica*
74	32	1327.4	Semi-fixed	7	1.68	0.79	0.86	*Agropyron mongolicum*
75	28	1328.1	Semi-fixed	6	1.61	0.77	0.90	*Artemisia ordosica*
76	30	1325.5	Semi-fixed	7	1.90	0.84	0.98	*Artemisia ordosica*
77	22	1325.9	Semi-fixed	3	0.51	0.26	0.46	*Artemisia ordosica*
78	23	1324.4	Semi-fixed	4	1.22	0.68	0.88	*Artemisia ordosica*
79	15	1325.0	Semi-fixed	5	1.20	0.60	0.75	*Chenopodium glaucum*
80	22	1324.4	Semi-fixed	5	1.33	0.68	0.83	*Agropyron mongolicum*
81	8	1325.0	Semi-fixed	4	0.99	0.54	0.71	*Agropyron mongolicum*
82	23	1324.1	Semi-fixed	2	0.48	0.30	0.70	*Artemisia ordosica*
83	18	1324.0	Semi-fixed	5	1.49	0.75	0.93	*Artemisia ordosica*
84	35	1319.0	Fixed-land	8	1.48	0.68	0.71	*Carex duriuscula*
85	22	1322.3	Fixed-land	4	1.18	0.64	0.85	*Agropyron mongolicum*
86	27	1322.0	Fixed-land	5	1.39	0.72	0.87	*Artemisia ordosica*
87	32	1324.0	Fixed-land	4	1.07	0.59	0.77	*Artemisia ordosica*
88	16	1324.0	Fixed-land	5	1.47	0.74	0.91	*Artemisia ordosica*
89	17	1325.0	Semi-fixed	5	1.39	0.72	0.87	*Artemisia ordosica*
90	15	1324.7	Semi-fixed	3	1.04	0.63	0.94	*Artemisia ordosica*
91	6	1326.0	Fixed-land	4	1.39	0.75	1.00	*Ulmus pumila*
92	33	1322.3	Fixed-land	4	1.23	0.68	0.89	*Agropyron mongolicum*
93	19	1337.0	Lowland	5	1.30	0.67	0.81	*Leymus chinensis*
94	45	1335.0	Lowland	8	1.63	0.74	0.79	*Cleistogenes caespitosa*
95	20	1330.0	Lowland	5	1.49	0.75	0.92	*Agropyron cristatum*

96	58	1327.0	Lowland	4	1.07	0.61	0.77	*Cleistogenes caespitosa*
97	19	1327.7	Lowland	5	1.27	0.65	0.79	*Asparagus schoberioides*
98	36	1328.0	Lowland	8	1.65	0.75	0.79	*Asparagus schoberioides*
99	29	1327.0	Lowland	8	1.80	0.80	0.87	*Cleistogenes caespitosa*
100	37	1327.0	Lowland	6	1.18	0.63	0.66	*Cleistogenes caespitosa*
101	28	1329.0	Lowland	5	1.28	0.66	0.80	*Thymus serpyllum*
102	36	1327.0	Lowland	5	1.42	0.72	0.88	*Artemisia frigida*
103	19	1326.0	Lowland	5	1.32	0.69	0.82	*Agropyron mongolicum*
104	28	1329.0	Lowland	6	1.64	0.79	0.92	*Artemisia ordosica*
105	17	1326.0	Lowland	5	1.36	0.70	0.84	*Cleistogenes caespitosa*
106	34	1326.0	Lowland	4	0.89	0.53	0.64	*Artemisia frigida*
107	37	1326.0	Lowland	5	1.52	0.76	0.94	*Agropyron mongolicum*
108	13	1336.0	Fixed-land	5	1.54	0.78	0.96	*Leymus chinensis*
109	8	1332.4	Fixed-land	4	1.04	0.60	0.75	*Leymus chinensis*
110	5	1326.2	Fixed-land	4	1.19	0.66	0.86	*Leymus chinensis*
111	7	1327.0	Fixed-land	5	1.44	0.73	0.89	*Leymus chinensis*
112	17	1325.6	Fixed-land	5	0.90	0.43	0.56	*Carex duriuscula*
113	7	1327.4	Fixed-land	4	1.21	0.67	0.87	*Leymus chinensis*
114	20	1326.7	Fixed-land	4	0.94	0.48	0.68	*Lappula myosotis*
115	6	1326.7	Fixed-land	4	1.29	0.70	0.93	*Leymus chinensis*
116	5	1324.0	Fixed-land	4	1.21	0.66	0.88	*Leymus chinensis*
117	17	1326.0	Fixed-land	4	0.45	0.19	0.32	*Carex duriuscula*
118	15	1326.0	Fixed-land	3	0.91	0.54	0.83	*Cleistogenes caespitosa*
119	20	1325.0	Fixed-land	4	1.30	0.71	0.94	*Thymus serpyllum*
120	11	1325.0	Fixed-land	4	1.03	0.55	0.75	*Carex duriuscula*
121	12	1324.6	Fixed-land	3	0.90	0.53	0.82	*Lappula myosotis*
122	29	1326.0	Fixed-land	6	0.92	0.45	0.51	*Carex duriuscula*

Table S2 The name, formula, and ecological meanings of spectral indices used in the present study

Order	Name	Formula	Ecological meanings	Reference
1	Anthocyanin Reflectance Index 1 (ARI1)	$ARI1 = \frac{1}{\rho_{550}} - \frac{1}{\rho_{700}}$	one measure of stressed vegetation	Gitelson et al., 2001
2	Anthocyanin Reflectance Index 2 (ARI2)	$AR12 = \rho_{800}\left[\frac{1}{\rho_{550}} - \frac{1}{\rho_{700}}\right]$	is a modification to the ARI1 that detects higher concentrations of anthocyanins in vegetation.	Liu et al., 2022
3	Atmospherically Resistant Vegetation Index (ARVI)	$ARVI = \frac{\rho_{800} - [\rho_{680} - \gamma(\rho_{450} - \rho_{680})]}{\rho_{800} + [\rho_{680} - \gamma(\rho_{450} - \rho_{680})]}$	an enhancement to the NDVI that is relatively resistant to atmospheric factors	Kaufman et al., 1992
4	Enhanced Vegetation Index (EVI)	$EVI = 2.5 * \frac{(NIR - Red)}{(NIR + 6 * Red - 7.5 * Blue + 1)}$	an improvement over NDVI by optimizing the vegetation signal in areas of high leaf area index	Huete et al., 2002
5	Green Atmospherically Resistant Index (GARI)	$GARI = \frac{NIR - [Green - \gamma(Blue - Red)]}{NIR + [Green - \gamma(Blue - Red)]}$	is more sensitive to a wide range of chlorophyll concentrations and less sensitive to atmospheric effects than NDVI.	Gitelson et al., 1996
6	Green Chlorophyll Index (GCI)	$GCI = \left(\frac{\rho_{NIR}}{\rho_{Green}}\right) - 1$	to estimate leaf chlorophyll content across a wide range of plant species.	Gitelson et al., 2003
7	Green Difference Vegetation Index (GDVI)	$GDVI = NIR - Green$	This index was originally designed with color-infrared photography to predict nitrogren requirements for corn.	Sripada et al., 2006
8	Green Leaf Index (GLI)	$GLI = \frac{(Green - Red) + (Green - Blue)}{(2 * Green) + Red + Blue}$	to measure wheat cover, where the red, green, and blue digital numbers (DNs) range from 0 to 255.	Louhaichi et al., 2001
9	Green Normalized Difference Vegetation Index (GNDVI)	$GNDVI = \frac{(NIR - Green)}{(NIR + Green)}$	This index was originally designed with color-infrared photography to predict nitrogren requirements for corn. This index is more sensitive to chlorophyll concentration than NDVI.	Gitelson et al., 1998

10	Green Optimized Soil Adjusted Vegetation Index (GOSAVI)	$GOSAVI = \frac{NIR - Green}{NIR + Green + 0.16}$	This index is similar to NDVI except that it measures the green spectrum from 540 to 570 nm instead of the red spectrum. This index is more sensitive to chlorophyll concentration than NDVI.	Sripada et al., 2006
11	Green Ratio Vegetation Index (GRVI)	$GRVI = \frac{NIR}{Green}$	sensitive to photosynthetic rates in forest canopies	Sripada et al., 2006
12	Green Soil Adjusted Vegetation Index (GSAVI)	$GSAVI = 1.5 * \frac{(NIR - Green)}{(NIR + Green + 0.5)}$	This index was originally designed with color-infrared photography to predict nitrogren requirements for corn. It is similar to SAVI, but it substitutes the green band for red.	Sripada et al., 2006
13	Green Vegetation Index (GVI)	$GVI = (-0.2848 * TM_1) \cdot (0.7243 * TM_4) + (0.0840 * TM_5) + (-0.1800 * TM_7) + (-0.2435 * TM_2) + (-0.5436 * TM_3) +$	This index minimizes the effects of background soil while emphasizing green 14vegetation	Kauthet al., 1976
14	Global Environmental Monitoring Index (GEMI)	$GEMI = eta(1 - 0.25 * eta) - \frac{Red - 0.125}{1 - Red}$	is similar to NDVI but is less sensitive to atmospheric effects.	Pinty et al., 1992
15	Infrared Percentage Vegetation Index (IPVI)	$IPVI = \frac{NIR}{NIR + Red}$	Like NDVI, is computationally faster. Values range from 0 to 1.	Crippen et al., 1990
16	Modified Chlorophyll Absorption Ratio Index (MCARI)	$MCARI = [(\rho_{700} - \rho_{670}) - 0.2(\rho_{700} - \rho_{550})] * (\rho_{700}/\rho_{670})$	This index indicates the relative abundance of chlorophyll.It is designed primarily to amplify the leaf-level chlorophyll signal, thereby indicating vegetation “physiological health and nutritional status,” rather than canopy structure or biomass.	Zarco-Tejada et al., 2005

17	Modified Chlorophyll Absorption Ratio Index Improved (MCARI2)	$MCARI2 = \frac{1.5[2.5(\rho_{800} - \rho_{670}) - 1.3(\rho_{800} - \rho_{550})]}{\sqrt{(2 * \rho_{800} + 1)^2 - (6 * \rho_{800} - 5 * \sqrt{\rho_{670}}) - 0.5}}$	This index can more accurately and consistently characterize the canopy's "green biomass" and its "gross primary productivity potential." It remains sensitive to variations in leaf area index even in dense, high-biomass stands where NDVI tends to saturate, and it minimizes the influence of changing chlorophyll concentrations	Haboudane et al., 2004
18	Modified Non-Linear Index (MNLI)	$MNLI = \frac{(NIR^2 - Red) * (1 + L)}{NIR^2 + Red + L}$	This index is an enhancement to the Non-Linear Index (NLI) that incorporates the Soil Adjusted Vegetation Index (SAVI)	Yang et al., 2021
19	Modified Soil Adjusted Vegetation Index 2 (MSAVI2)	$MSAVI2 = \frac{2 * NIR + 1 - \sqrt{(2 * NIR + 1)^2 - 8(NIR - Red)}}{2}$	It reduces soil noise and increases the dynamic range of the vegetation signal.	Qi et al., 1994
20	Modified Triangular Vegetation Index (MTVI)	$MTVI = 1.2[1.2(\rho_{800} - \rho_{550}) - 2.5(\rho_{670} - \rho_{550})]$	suitable for LAI estimations	Haboudane et al., 2004
21	Modified Triangular Vegetation Index - Improved (MTVI2)	$MTVI2 = \frac{1.5[\rho_{800} - \rho_{550} - 2.5(\rho_{670} - \rho_{550})]}{\sqrt{(2 * \rho_{800} + 1)^2 - (6 * \rho_{800} - 5 * \sqrt{\rho_{670}}) - 0.5}}$	a better predictor of green LAI	Eitelet al., 2007
22	Normalized Difference Mud Index (NDMI)	$NDMI = \frac{(\rho_{795} - \rho_{990})}{(\rho_{795} + \rho_{990})}$	This index highlights muddy or shallow water pixels	Liu et al., 2022
23	Optimized Soil Adjusted Vegetation Index (OSAVI)	$OSAVI = \frac{(NIR - Red)}{(NIR + Red + 0.16)}$	is best used in areas with relatively sparse vegetation	Peng et al., 2018
24	PCA-cv		Coefficients of variation in principle components	
25	Renormalized Difference Vegetation Index (RDVI)	$RDVI = \frac{(NIR - Red)}{\sqrt{(NIR + Red)}}$	to highlight healthy vegetation	Roujean et al., 1995
26	Red Green Ratio Index (RGRI)	$RGRI = \frac{\sum_{i=600}^{599} R_i}{\sum_{j=500}^{599} R_j}$	indicates the relative expression of leaf redness caused by anthocyanin to that of chlorophyll.	Gamon et al., 1999
27	Soil Adjusted Vegetation Index (SAVI)	$SAVI = \frac{1.5 * (NIR - Red)}{(NIR + Red + 0.5)}$	This index is best used in areas with relatively sparse vegetation	Huete et al., 1988

28	Sum Green Index (SGI)	SGI is the mean of reflectance across the 500 nm to 600 nm portion of the spectrum.	This index is used for detecting changes in vegetation greenness.	Lobell et al., 2003
29	Transformed Chlorophyll Absorption Reflectance Index (TCARI)	$TCARI = 3\left[(\rho_{700} - \rho_{670}) - 0.2(\rho_{700} - \rho_{550})\left(\frac{\rho_{700}}{\rho_{670}}\right)\right]$	This index indicates the relative abundance of chlorophyll.It is highly sensitive to chlorophyll concentration; by amplifying the chlorophyll absorption trough, it rapidly and quantitatively reflects vegetation nitrogen status and early physiological stress.	Haboudane et al., 2004
30	Transformed Difference Vegetation Index (TDVI)	$TDVI = 1.5\left[\frac{(NIR - Red)}{\sqrt{NIR^2 + Red + 0.5}}\right]$	for monitoring vegetation cover in urban environments.	Bannari et al., 2002
31	Triangular Greenness Index (TGI)	$TGI = \frac{(\lambda_{\text{Red}} - \lambda_{\text{Blue}})(\rho_{\text{Red}} - \rho_{\text{Green}}) - (\lambda_{\text{Red}} - \lambda_{\text{Green}})(\rho_{\text{Red}} - \rho_{\text{Blue}})}{2}$	it is suitable for RGB cameras.	Raymond et al., 2011
32	Visible Atmospherically Resistant Index (VARI)	$VARI = \frac{Green - Red}{Green + Red - Blue}$	to estimate the fraction of vegetation in a scene	Gitelson et al., 2002
33	Wide Dynamic Range Vegetation Index (WDRVI)	$WDRVI = \frac{(a * NIR - Red)}{(a * NIR + Red)}$	is more sensitive to a wider range of vegetation fractions and to changes in LAI.	GITELSON et al., 2004
34	WorldView Improved Vegetative Index(WIVI)	$WIVI = \frac{(NIR2 - Red)}{(NIR2 + Red)}$	The common range for green vegetation.	Wolf et al., 2010
35	WorldView Non-Homogeneous Feature Difference (WNHFD)	$WNHFD = \frac{(Red\ Edge - Coastal)}{(Red\ Edge + Coastal)}$	to identify features that contrast highly against the background.	Wolf et al., 2010

Reference

Bannari, A., Asalhi, H., and Teillet, P. M., 2002. Transformed difference vegetation index (TDVI) for vegetation cover mapping. Proc. IEEE Int. Geosci. Remote Sens. Symp. (IGARSS 2002), Toronto, ON, Canada, 24–28 June 2002, Vol. 5: 3053–3055.

Crippen, R. E., 1990. Calculating the vegetation index faster. Remote Sens. Environ. 34(1): 71–73. https://doi.org/10.1016/0034-4257(90)90009-3

Eitel, J. U. H., Long, D. S., Gessler, P. E., and Smith, A. C., 2007. Using in-situ measurements to evaluate the new RapidEye™ satellite series for prediction of wheat nitrogen status. Remote Sens. Environ. 108(2–3): 4183–4190. https://doi.org/10.1016/j.rse.2007.08.013

Gamon, J. A., Surfus, J. S., 1999. Assessing leaf pigment content and activity with a reflectometer. New Phytol. 143: 105–117. https://doi.org/10.1046/j.1469-8137.1999.00480.x

Gitelson, A. A., Merzlyak, M., 1998. Remote Sensing of Chlorophyll Concentration in Higher Plant Leaves. Adv. Space Res. 22(5): 689–692. https://doi.org/10.1016/S0273-1177(98)00144-8

Gitelson, A. A., Gritz, Y., Merzlyak, M. N., 2003. Relationships between leaf chlorophyll content and spectral reflectance and algorithms for non-destructive chlorophyll assessment in higher plant leaves. Plant Physiol. 160(3): 271–282. https://doi.org/10.1071/PP02082

Gitelson, A. A., Kaufman, Y. J., Merzlyak, M. N., 1996. Use of a green channel in remote sensing of global vegetation from EOS-MODIS. Remote Sens. Environ. 58(3): 289–298. https://doi.org/10.1016/0034-4257(96)00042-7

Gitelson, A. A., Merzlyak, M. N., Chivkunova, O. B., 2001. Optical properties and nondestructive estimation of anthocyanin content in plant leaves. Photochem. Photobiol. 74(1): 38–45. https://doi.org/10.1562/0031-8655(2001)074[0038:OPANEO]2.0.CO;2

Gitelson, A. A., 2004. Wide dynamic range vegetation index for remote quantification of biophysical characteristics of vegetation. J. Plant Physiol. 161(2): 165–173. https://doi.org/10.1078/0176-1617-01084

Haboudane, D., Miller, J. R., Pattey, E., and Smith, A. C., 2004. Hyperspectral vegetation indices and novel algorithms for predicting green LAI of crop canopies: Modeling and validation in the context of precision agriculture. Remote Sens. Environ. 90(3): 337–352. https://doi.org/10.1016/j.rse.2004.01.011

Huete, A. R., Didan, K., Miura, T., and Smith, A. C., 2002. Overview of the radiometric and biophysical performance of the MODIS vegetation indices. Remote Sens. Environ. 83: 195–213. https://doi.org/10.1016/S0034-4257(02)00096-2

Huete, A. R., 1988. A soil-adjusted vegetation index (SAVI). Remote Sens. Environ. 25(3): 295–309. https://doi.org/10.1016/0034-4257(88)90106-X

Kaufman, Y. J., Tanré, D., 1992. Atmospherically Resistant Vegetation Index (ARVI) for EOS-MODIS. IEEE Trans. Geosci. Remote Sens. 30(2): 261–270. https://doi.org/10.1109/36.129241

Kauth, R. J., 1976. Tasselled Cap—A Graphic Description of the Spectral-Temporal Development of Agricultural Crops as Seen by Landsat. LARS Symp.: 41–51. https://ageconsearch.umn.edu/record/222424

Liu, L. X., Pang, Y., Sang, G. Q., and Smith, A. C., 2022. Applying high resolution remote sensing to access tree species diversity of monsoonal broad-leaved evergreen forest in Puer City. Acta Ecol. Sin. 42(20): 8398–8410. https://doi.org/10.5846/stxb202106231710

Lobell, D., Asner, G., 2003. Hyperion Studies of Crop Stress in Mexico. Proc. 12th Annu. JPL Airborne Earth Sci. Workshop, Pasadena, CA. https://earth.jpl.nasa.gov/files/airs2003_abstracts.pdf

Louhaichi, M., Borman, M. M., Johnson, D. E., 2001. Spatially Located Platform and Aerial Photography for Documentation of Grazing Impacts on Wheat. Geocarto Int. 16: 65–70. https://doi.org/10.1080/10106040108544267

Peng, Y., Fan, M., Song, J. Y., and Smith, A. C., 2018. Assessment of plant species diversity based on hyperspectral indices at a fine scale. Sci. Rep. 8: 4776. https://doi.org/10.1038/s41598-018-23183-5

Pinty, B., Verstraete, M., 1992. GEMI: a Non-Linear Index to Monitor Global Vegetation From Satellites. Vegetatio 101(1): 15–20. https://doi.org/10.1007/BF00044317

Qi, J., Chehbouni, A., Huete, A. R., Kerr, Y. H., and Sorooshian, S., 1994. A modified soil adjusted vegetation index. Remote Sens. Environ. 48(2): 119–126. https://doi.org/10.1016/0034-4257(94)90134-1

Raymond Hunt, E., Daughtry, C. S. T., Eitel, J. U. H., and Smith, A. C., 2011. Remote sensing leaf chlorophyll content using a visible band index. Agron. J. 103(4): 1090–1099. https://doi.org/10.2134/agronj2010.0477

Roujean, J.-L., Breon, F.-M., 1995. Estimating PAR absorbed by vegetation from bidirectional reflectance measurements. Remote Sens. Environ.

51(3): 375–384. https://doi.org/10.1016/0034-4257(95)00048-4

Sripada, R. P., Heiniger, R. W., White, J. G., and Smith, A. C., 2006. Aerial Color Infrared Photography for Determining Early In-Season Nitrogen Requirements in Corn. Agron. J. 98(4): 968–977. https://doi.org/10.2134/agronj2005.0146

Wolf, A., 2010. Using WorldView 2 Vis-NIR MSI Imagery to Support Land Mapping and Feature Extraction Using Normalized Difference Index Ratios. Unpublished Report, Longmont, CO: DigitalGlobe. Available from: https://www.maxar.com/sites/default/files/documents/worldview-2-imagery-land-mapping.pdf

Yang, Z., Willis, P., and Mueller, R., 2008. Impact of band-ratio enhanced AWiFS image on crop classification accuracy. Proc. 2008 ASPRS Annu. Conf., Portland, OR, USA, 28 April–2 May 2008. https://www.asprs.org/wp-content/uploads/pers/2008conference/proceedings/0295.pdf

Zarco-Tejada, P. J., Ustin, S., Whiting, M., 2005. Temporal and spatial relationships between within-field yield variability in cotton and high-spatial hyperspectral remote sensing imagery. Agron. J. 97: 641–653. https://doi.org/10.2134/agronj2004.0148